


RESEARCH ARTICLE

Flutter assessment of a rotor blade in hover based on indicial aerodynamics considering blade aerofoil, rotor inflow and wake periodicity

J. Arnold 

DLR German Aerospace Center, Göttingen, Germany
Email: Juergen.Arnold@dlr.de

Received: 1 March 2022; **Revised:** 21 March 2024; **Accepted:** 20 August 2024

Keywords: articulated rotor blade; multibody dynamics; indicial aerodynamics; blade flutter

Abstract

The experimental 7AD rotor blade is assessed for flutter stability in hover to identify the influence of aerodynamic contributions related to blade aerofoil, rotor inflow and wake periodicity on flutter onset. For the aeroelastic analyses, the multibody model is tightly coupled with an unsteady aerodynamic model based on Wagner's function and related enhancements for the general motion of an aerofoil section considering heave and pitch. The mathematical setup of the approximated Wagner function in state space is extended for axial flow to include unsteady effects related to rotor inflow and wake periodicity. Since the aerodynamic model is based on indicial response functions, a separation of these contributions is possible and allows for the study of their impact on rotor blade flutter. The according flutter results are extracted in terms of frequency and damping behaviour for three test cases that differ in the unsteady aerodynamic model for circulation comprising blade aerofoil, rotor inflow and wake periodicity. As known for articulated rotor blades, also the 7AD blade exhibits a classical bending-torsion coupling. The lowest flutter onset is found for unsteady aerodynamics limited to blade aerofoil, whilst the cases with added rotor inflow and wake periodicity show both the same flutter onset at a 5% larger rotor speed. Here, the influence of rotor inflow plays the major role, since it increases the torsion damping within the critical flutter coupling. Added wake periodicity neither changes frequency nor damping and, hence, does not affect the aeroelastic coupling.

Abbreviations:

CFD	Computational Fluid Dynamics
CSD	Computational Structural Dynamics
DAE	Differential Algebraic Equation
FEM	Finite Element Method
GVT	Ground Vibration Test
LTI	Linear Time Invariant
MBS	Multibody System
ODE	Ordinary Differential Equation
UFEL	User Force Element
UPM	Unsteady Panel Method

Nomenclature

B, D, K	Jacobian matrices
C_T	Thrust coefficient
G	Constraint matrix

This paper is a version of a presentation given at the 47th RAeS European Rotorcraft Forum 2021.

M	Mass matrix
N_b	Number of blades
U	Velocity
b	Semichord
f	Force vector, frequency, function
k	Reduced frequency
q	Generalised coordinates
r	Radial station
t	Time
u	System input
Ω	Angular velocity
λ	Lagrange multiplier
λ_i	Inflow
τ	Reduced time
Φ	Indicial response function
ω	Pitch angular velocity

1.0 Introduction

The analysis of rotor blade flutter has to consider all major physical couplings which are relevant for the rotating system. This requires the accurate representation of centrifugal stiffening and gyroscopic coupling effects for the dynamic system as well as the interaction of the rotor wake with the unsteady aerodynamic forces on the rotor blades in hover and forward flight. While the pitch-flap coupling dominates the flutter behaviour of the articulated rotor blade with blade hinges, the hingeless rotor concept exhibits an additional flutter mechanism which is driven by the coupling of lagwise and flapwise blade motion due to rotational effects resulting in a subsequent kinematic change of blade pitch [1]. By placing the centres of mass of the individual sections in the aerodynamic centre on the blade axis at quarter chord and providing mechanical lead-lag damping, the straight rotor blade is usually not flutter critical. Earlier flutter approaches considered the rotor blade as rigid in terms of pitch and flap motion and thus, could reduce the flutter task to an investigation of the control stiffness and the chordwise mass balance [2]. The introduction of new rotor concepts and optimised blade shapes [3] require more knowledge on possible flutter couplings in advance and freedom from flutter must be demonstrated in a wider context. In particular, the innovative blade shapes with forward and backward sweep, feature the possibility of new aeroelastic couplings. This is due to their flap bending modes contributing substantial shares in blade twist [4]. Here, the assumption of rigid blades is not sufficient, and the investigation of pitch-flap stability has to further consider the bending-torsion coupling of the flexible rotor blade. Other factors [2] influencing the pitch-flap stability comprise the shed wake influence leading to a slight modification of the flutter boundary, wake-excited flutter introducing a single-degree-of-freedom instability for operating conditions at low collective pitch, influence of forward flight with periodic coefficients for medium to large advance ratios, coupled blades through the rotor control system and elastic rotor shaft as well as additional degrees-of-freedom as found for example with flexible rotor blades. Finally, stall flutter [5] is present for large advance ratios in the fast forward flight and related to an amplified pitch motion of the retreating rotor blade due to high and alternating torsional load peaks under dynamic stall condition.

Numerical methods in time domain and system analysis via linearisation are used to study flutter stability. Examples comprise known comprehensive codes like CAMRAD II [6] and HOST [7]. In general, the equations of motion are linearised for the trimmed rotor and then subjected to analysis of the eigenbehaviour in terms of a classic stability rating by checking damping values. This approach is valid for time invariant system matrices and thus, is limited to symmetric rotors with axial inflow as found in hover condition. For general rotating systems (e.g. unsymmetric rotor, forward flight) linearisation leads to linear time periodic system matrices which no longer permit a stability assessment based on eigenvalue analysis. At this point the Floquet method and modern enhancements or multiblade coordinates are applied [2]. Another possibility is the evaluation of decay behaviour after the excitation of the

Table 1. Multi-fidelity unsteady aerodynamics for coupled rotor simulations with MBS SIMPACK

Fidelity Level	Coupling	Aerodynamics	Duration	Discretization
Low	UFEL-MBS	Wagner++	Sec-Min / Rev	Blade strip
Mid	UPM-MBS	UPM	Min-Hrs / Rev	Surface panel
High	CFD-MBS	TAU	Days / Rev	Volume

rotor system by means of direct numerical integration in the time domain, which takes account of all non-linearities of the modelling. To this, a strong CFD-CSD coupling together with the moving block method [8] can be applied. Next to the use of high-fidelity aerodynamics from CFD, a major improvement of the overall prediction capability for the aeromechanic simulation of rotorcraft is available by means of a multibody system (MBS) for the setup of the dynamic model [9, 10] which is characterised by connected rotary and non-rotary substructures. The application of multibody dynamics allows the consideration of all non-linear contributions relevant in a rotating system like geometric stiffening of the flexible blades and additional damping terms activated by gyroscopic effects as well as the provision of a correct mechanical interface between the rotating and non-rotating frames by applying non-linear joint definitions. Recent efforts have improved elastic multibody models within the comprehensive simulation by introducing three-dimensional solid structures in the coupled simulation within HELIOS [11] and sophisticated beam models in VAST [12].

In the presented work, the multibody system SIMPACK [13, 14] is used for the setup and simulation of the dynamic model of the 7AD rotor with its flexible blades. Flexibility of the non-rotating blade is described in the multibody system SIMPACK with a modal approach for available finite element models. For the assessment of the rotor in axial inflow condition, an unsteady theory using indicial aerodynamics based on the extended Wagner function from section 2.2 in combination with steady two-dimensional aerofoil data is applied to the multibody model. This approach allows an efficient and robust flutter assessment of DLR rotor setups in the design process and before entry into service, but was so far limited to hover and has been recently expanded to steady axial flight [15]. According to Table 1, it provides the low-fidelity solution within the choice of three aerodynamic methods for the MBS rotor analysis, which form a multi-fidelity aerodynamic approach around a high-fidelity dynamic model as common basis. Hence, the rotor simulation can be adjusted to the required accuracy with a factor of between 50 to 100 in computational time from one fidelity level to the other. Since the approximated Wagner function and the extensions for axial flow are available in a state space model, the evaluation is possible in the time domain or by linearisation. Here, linearised results are available in terms of frequency and damping behaviour allowing for an initial frequency placement and stability check of the isolated rotor.

The 7AD rotor was included in several European wind tunnel campaigns and operated in different setups as isolated or main rotor of a complete helicopter configuration. Also, the known GOAHEAD experimental setup [16] in the DNW-LLF wind tunnel from Fig. 1 made intensive use of the articulated rotor. This article summarises the aeroelastic modelling and steps performed towards an improved flutter assessment of the 7AD rotor model in hover utilising a multibody system. The objective is the stability assessment of the elastic rotor blade using tight coupling between the multibody system and an unsteady aerodynamic model for rotor blade sections based on indicial response functions [17] which capture the transient changes in aerodynamic variables within the Duhamel superposition integral. The aerodynamic model has been developed at the DLR Institute of Aeroelasticity and applied for the stability analyses of isolated rotor setups with straight [18] and double-swept rotor blades [19] in the DLR projects FAST- and



Figure 1. 7AD rotor in the GOAHEAD setup.

URBAN-Rescue [20] before test entry using the basic Wagner function in state space. Furthermore, an earlier contribution [4] dealt with the flutter assessment of the isolated 7AD rotor in hover with the same aerodynamics and the available MBS model now forms the basis for the application of the new unsteady aerodynamic model, which is predicated on the extended Wagner function for axial rotor flow. The extension closes the gap for indicial response functions in terms of a description in state space for hover flight enabling the linearisation of the isolated aeroelastic rotor to extract basic rotor frequencies and damping values. Here, the use of indicial response functions allows to separate unsteady aerodynamic effects related to blade aerofoil, rotor inflow as well as rotor wake periodicity and to understand how they influence flutter onset of the 7AD rotor blade.

2.0 Numerical methods

2.1 Multibody dynamics

The multibody system SIMPACK [13, 14] is used to set up and simulate the dynamic model of the rotor with its flexible rotor blades including large rigid body motions of the rotor hub and blade hinges as well as small deformations of the elastic structure. The development of the simulation package was originally initiated by DLR and later out-sourced for further development and commercial distribution.

SIMPACK is a general, non-linear three-dimensional multibody simulation tool and allows dynamic models for rotating and non-rotating systems consisting of rigid and elastic bodies to be built. The degrees-of-freedom are represented by a number of independent state variables [21] that define the motion of each body. In describing the kinematic behaviour, the motion or the position of the multibody system is studied with respect to the kinematic joints. Here, non-linear joint definitions provide the correct coupling of the bodies and introduce contributions from rotation w.r.t. stiffness and damping effects. For further modelling a huge element library for joints, force elements and other features is available. Also user force elements (UFEL) can be used to add dynamics by introducing ordinary differential equations (ODE) in terms of state space models, as done in this work for the indicial aerodynamics from section 2.2. Next to the simulation in time domain, the possibility of linearisation allows the system analysis by investigating the frequency and damping content. Here, the state space representation of the linear and time invariant system (LTI) is applied to derive the eigenbehaviour of the system.

If a dynamic multibody system is described by a minimum set of generalised coordinates $q(t)$, the equations of motion form a set of non-linear second-order ODE [22] as given by

$$M(q) \cdot \ddot{q}(t) = f(q, \dot{q}, t) \quad (1)$$

with the mass matrix $M(q)$ containing mass and inertia properties of all bodies as well as the vector of applied and gyroscopic forces $f(q, \dot{q}, t)$ which depends on simulation time t . The equations of motion from Equation (1) can be also transferred into a generic state space form. If complex kinematics with constraints, connections in closed kinematic loops (see Fig. 2) or time-discrete state equations from discrete force and control elements need to be handled, the system motion is described by second-order differential-algebraic equations (DAE) with

$$M(q) \cdot \ddot{q}(t) = f(q, \dot{q}, t) - G^T(q, t) \cdot \lambda(t) \quad (2)$$

including the constraint forces $-G^T(q, t) \cdot \lambda(t)$ that are determined by the constraint matrix $G(q, t)$ and Lagrange multipliers $\lambda(t)$.

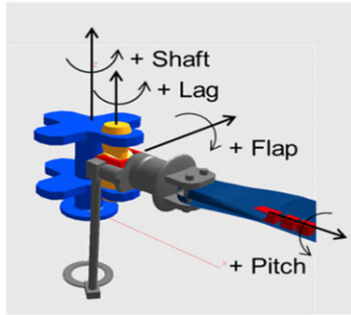


Figure 2. 7AD rotor hub with articulated blade and closed kinematic loop to the swash plate.

Flexibility of the non-rotating blade is described in the multibody system SIMPACK either with a modal approach [23, 24] for available finite element models or on the basis of an intrinsic beam model. The following options allow the introduction of elastic rotor blades [14]:

- (A) Implementation of complete elastic blade as one elastic body and additional geometric stiffness terms via standard FlexModal interface
- (B) Implementation of elastic blade with connected elastic substructures via standard FlexModal interface
- (C) Application of the intrinsic elastic beam model SIMBEAM
- (D) Application of the rotor blade generator based on SIMBEAM

Option (A) enables the straight-forward use of finite element models of industrial model size. Currently, the FlexModal interface supports ABAQUS, ANSYS, MSC.NASTRAN, NX.NASTRAN, PERMAS and RADIOSS. The option (B) is advantageous to add further non-linear characteristics of the multibody joints that interconnect elastic substructures along the rotor blade. For beam models [25], it can be easily combined with option (A). In addition, option (C) and (D) provide a solution, if a finite element code is not available or is not supported by FlexModal. In the present work, SIMPACK 2021 was used.

Option (A) which is based on the implementation of the complete elastic model together with additional geometric stiffness using the FlexModal interface is chosen for the 7AD rotor blades. Two FEM solutions from a preprocessing step with the finite element code MSC.NASTRAN are required in order to process the blade:

- A modal solution provides the modal elastic model with natural frequencies and mode shapes for the non-rotating blade at $\Omega = 0$ rad/s.
- A static solution provides the geometric stiffness terms for the description in the relevant degrees-of-freedom of the rotating blade for $\Omega > 0$ rad/s (centrifugal forces due to angular velocity).

FlexModal reads the model geometry, mass and stiffness matrices, natural frequencies, mode shapes, geometric stiffening terms and the used load case entries for the derivation of the geometric stiffening terms from the pre-processed finite element data. FlexModal then translates this input into a common flexibility description which is based on the standard input data (SID) format as described in Ref. [24]. The file containing the flexible substructure is added in SIMPACK with marker locations which are the same as found at the node positions in the finite element model, changing a rigid into an elastic body. Regarding aspects of component modal synthesis and substructuring, any hybrid model consisting of rigid and flexible bodies can be built. Rigid bodies can be replaced by flexible ones by introducing a modal elastic model as described above or spring stiffness can be applied to a joint between two bodies from the MBS element library. SIMPACK adds the additional equations for the modal degrees-of-freedom to the set of DAE and solves the resulting equations.

2.2 Indicial aerodynamics

The unsteady aerodynamic model for rotor blade sections takes advantage of indicial response functions [17], which capture the transient changes in aerodynamic variables within the Duhamel superposition integral. These functions model the unsteady aerodynamic response in time domain for variations in angle-of-attack and/or axial inflow. The model is based on Wagner's function [17] in combination with steady two-dimensional aerofoil data and applied to the multibody model. This function considers a two-dimensional thin aerofoil in impulsive motion from rest to uniform velocity U and is commonly used as a model for the circulatory lift development related to a change in angle-of-attack with fixed wing problems. According to Fung [26], the description of unsteady lift is extended from an impulsive to general motion including both pitch and heave motion by taking unsteady apparent mass terms for non-circulatory effects into account.

The fast aerodynamic model is based on radial independent strips and has been implemented using the approximation of R.T. Jones [18, 19] for Wagner's function $\Phi(\tau)$ with

$$\Phi(\tau) = 1 - 0.165e^{-0.0455\tau} - 0.335e^{-0.300\tau} \quad \text{where } \tau = U \cdot t/b \quad (3)$$

represents the non-dimensional reduced time. According to Equation (3), Wagner's function describes the unsteady lift development towards the steady-state value for increasing distance τ traveled in semichords b during time t . The approximation is shown in Fig. 3 together with values from the state space formulation of Wagner's function in the SIMPACK UFEL.

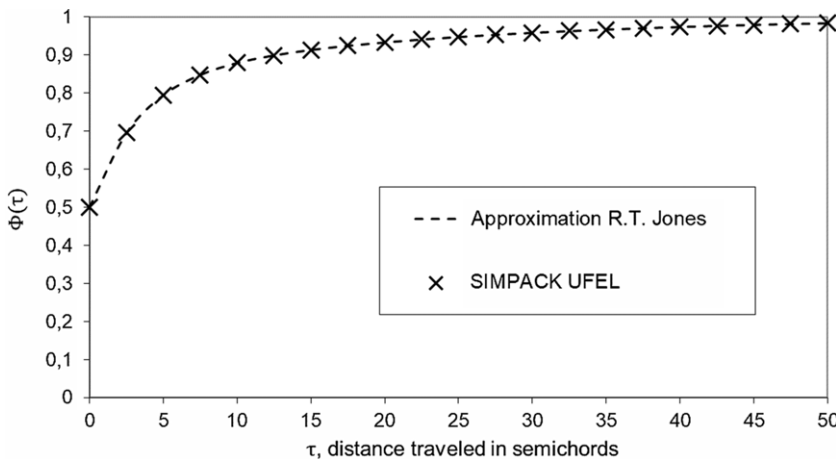


Figure 3. Wagner's function for an incompressible fluid.

All indicial response functions affect the circulatory part of the unsteady lift, are implemented in terms of a state space model in the SIMPACK force element and extended for rotors under axial flow condition. Related contributions include blade aerofoil from the Wagner function [27], axial dynamic inflow from a non-linear differential equation [17] derived out of the results gained by Carpenter and Fridovich [28], and wake periodicity as modelled in Loewy's function [29] by a complex factor. The associated expressions for axial dynamic inflow and wake periodicity are listed as Equations (4) and (5), respectively. They introduce the rotor parameters of rotor angular velocity Ω , inflow λ_i , thrust coefficient C_T , pitch angular velocity ω and number of blades N_b . All circulatory contributions are accounted for by three dynamic states per radial strip, which can be configured in the model setup.

$$\left(\frac{0.849}{\Omega}\right) \cdot \dot{\lambda}_i + 2 \cdot \lambda_i^2 = C_T \quad (4)$$

$$e^{i \cdot 2\pi \cdot \omega / (N_b \cdot \Omega)} = \cos\left(\frac{2\pi \cdot \omega}{N_b \cdot \Omega}\right) + i \cdot \sin\left(\frac{2\pi \cdot \omega}{N_b \cdot \Omega}\right) \quad (5)$$

The fundamental solution of Equation (4) is found from integral tables for rational functions [30] and leads to a kernel expression $\lambda_i(t) = f(C_T, \Phi_\lambda)$ for dynamic inflow [31] that contains the axial inflow function $\Phi_\lambda(\tau_\lambda)$ with

$$\Phi_\lambda(\tau_\lambda) = 1 - e^{-3.3315 \cdot \tau_\lambda} \quad \text{where } \tau_\lambda = \sqrt{C_T} \cdot \Omega \cdot t \quad (6)$$

represents the non-dimensional reduced time depending on rotor parameters. This function is a measure for the inflow change related to a pitch input and introduces a transition effect into the kernel expression with a similar curve shape as depicted in Fig. 3 for Wagner's function, but ranging from zero to one. Since the mathematical setup of the axial inflow function resembles Equation (3), it can be iteratively solved together with the approximated Wagner function to adapt the motion induced lift from Wagner in terms of the thrust input for the inflow induced lift from the axial inflow function.

The influence of added rotor inflow on the development of unsteady lift is obtained by applying pitch step excitations in the SIMPACK force element and evaluating the temporal development for the angle-of-attack which is a measure for lift and can be compared to the pitch input. Here, the indicial response for the Wagner function and axial dynamic inflow interacts at each radial station r depending on two separate scales for reduced time, namely τ and τ_λ . The contribution of Wagner's function with τ (rotor in-plane dynamics related to $U = \Omega \cdot r$) reaches the steady state in physical time earlier than the one of axial inflow with τ_λ (rotor out-of-plane dynamics related to $\sqrt{C_T} = \sqrt{2 \cdot \lambda_i}$). As illustrated in Fig. 4 for a two-bladed rotor, dynamic axial inflow reduces the effective angle-of-attack for the rotor section, whilst a wing section without inflow follows the basic Wagner function and reaches the commanded pitch angle. Hence, the onset of rotor inflow decreases the angle-of-attack towards a steady value which represents the so-called lift deficiency [32] of a rotor under axial inflow. To complete the extension of Wagner's function to axial rotor flow, the periodicity term from Loewy's function [29] is implemented in the state space model, which was carefully tested for harmonic pitch oscillation to gain aerodynamic transfer functions for comparison of the basic Wagner function with the extended models. Figure 5 shows the lift amplitudes and phase angles versus rotor harmonics for the radial section r of a four-bladed rotor ($\Omega = 62.83$ rad/s, $r = 1.0$ m, $b = 0.05$ m, $C_{T0} = 0.008263$) oscillating around mid chord. The influence of inflow and periodicity related to 4/rev can be seen in both lift amplitude and phase angle. As predicted by Loewy, reduced damping is found due to a smaller amplitude [1, 2] and a less negative angle for multiples of the blade passing frequency, i.e. 4/rev and 8/rev. For the used parameters, 1/rev equals a reduced frequency of $k = 0.05$ which is defined as:

$$k = \omega \cdot b / U \quad \text{with} \quad U = \Omega \cdot r \quad (7)$$

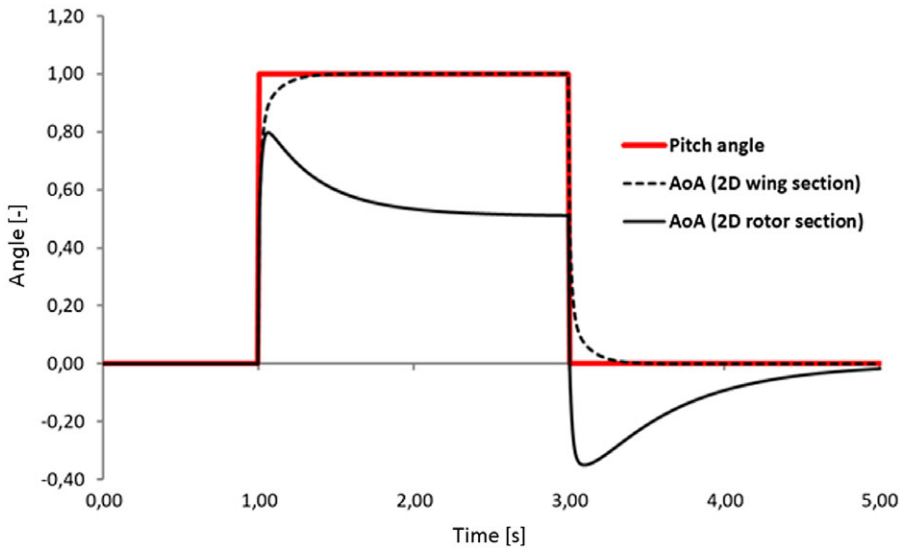


Figure 4. Temporal development of angle-of-attack (AoA) for pitch step input due to axial inflow dynamics.

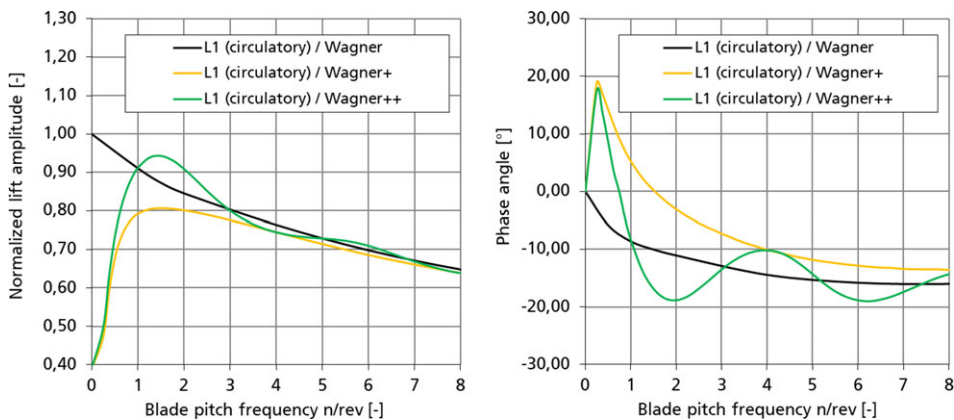


Figure 5. Unsteady lift amplitudes and phase angles of a four-bladed rotor obtained with Wagner function and extensions for rotor inflow (+) and wake periodicity (++).

2.3 Aeroelastic assessment

Standard features in MBS SIMPACK allow the aeroelastic assessment in a tightly coupled manner on equation level of the rotor blades for axial inflow condition in time domain and by using linearised results. In the latter approach which is based on linearisation, consecutive analysis of the eigenbehaviour and stability rating from damping values can be followed here, since the system matrices for the symmetric rotor with axial inflow remain time invariant and the unsteady aerodynamic forces are considered in the dynamic state set. The analysis is performed with the intrinsic eigensolver and delivers typical flutter results in terms of frequency and damping plots. In general, these results allow the verification of frequency placement and stability for the aeroelastic rotor system.

According to Ref. [22], the linearisation of the equations of motion from Equation (1) is the key to the linear stability and eigenmode analysis close to an equilibrium and to other methods of linear system

analysis. Writing the right-hand side for the vector of applied and gyroscopic forces as $f(q, \dot{q}, u(t))$ with system inputs $u(t)$ the linearisation about an equilibrium given by $q(t) = q^*$, $\dot{q} = 0$, $u = 0$ yields

$$M(q^*) \cdot \ddot{q} = -D \cdot \dot{q} - K \cdot q + B \cdot u(t) \quad \text{with} \quad D = -\frac{\partial f}{\partial \dot{q}}(q^*, 0, 0), \quad K = -\frac{\partial f}{\partial q}(q^*, 0, 0) \quad (8)$$

$$\text{and} \quad B = \frac{\partial f}{\partial u}(q^*, 0, 0)$$

where the Jacobians $\partial f/\partial q$, $\partial f/\partial \dot{q}$ and $\partial f/\partial u$ are approximated by classical finite differences.

3.0 Models and results

3.1 Dynamic and aerodynamic models

The mechanical setup of the 7AD rotor system is depicted in Fig. 6 and consists of the flexible rotor blades and a rigid model for the DLR-ONERA rotor hub that is improved with measured values [33] for pitch link and lagging spring stiffness as well as lagging damping. As shown in Fig. 2, the rotor hub is modelled with SIMPACK features to close the kinematic loop composed of lead-lag hinge, flap hinge and pitch bearing via the pitch link to the swash plate. The flexibility of the non-rotating blade is described in the multibody system with a modal approach from a real modes solution and additional geometric stiffness contributions for the rotating blade are considered by static load cases for the relevant degrees of freedom, both computed in a preprocessing step with the finite element software MSC.NASTRAN. Furthermore, the centrifugal pitching moment is considered at each radial marker via a SIMPACK Expression. The four bladed rotor has a diameter of 4.2m, mean blade chord of 0.14m and a solidity of 0.085. Both the flap and lead-lag hinges are located at a radius of 0.075m and the blade attachment is found at the radial station of 0.275m. The blade mass is approximately 3.18kg. Figure 7 shows the MSC.NASTRAN beam model of the 7AD rotor blade along the straight blade axis and curved blade tip with additional rigidly connected nodes to model trailing and leading edge positions.

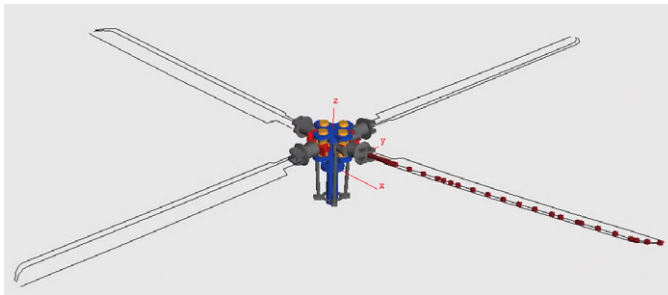


Figure 6. Multibody model of articulated 7AD rotor.

As described in a previous study [4], measured vibration data is available from a ground vibration test (GVT) with rowing hammer technique for the clamped blade comprising modal properties in terms of natural frequencies and mode shapes for the non-rotating 7AD rotor blade. The comparison of simulation results for the clamped beam model with the experimental modal data takes the measured frequencies into account and global stiffness parameters of the finite element models are adjusted with respect to modulus of elasticity and shear, if necessary. The natural frequencies for the elastic blade modes obtained with the finite element and multibody model are given in Table 2 in terms of a relative frequency deviation with respect to the GVT results as reference values.

Table 2. Comparison of calculated frequencies with GVT data for clamped rotor blade (normalised to f_{GVT})

Mode	f_{GVT} [-]	f_{FEM} [-]	f_{MBS} [-]
1 / F1	1.000	0.980	0.980
2 / L1	1.000	1.009	1.009
3 / F2	1.000	1.015	1.015
4 / F3	1.000	0.991	0.991
5 / T1	1.000	0.996	0.996
6 / F4	1.000	1.034	1.034
7 / L2	1.000	1.062	1.062
8 / F5	1.000	1.004	1.004
9 / F6	1.000	0.995	0.995
10 / T2	1.000	0.959	0.959
(F = flap mode / L = lag mode / T = torsion mode)			

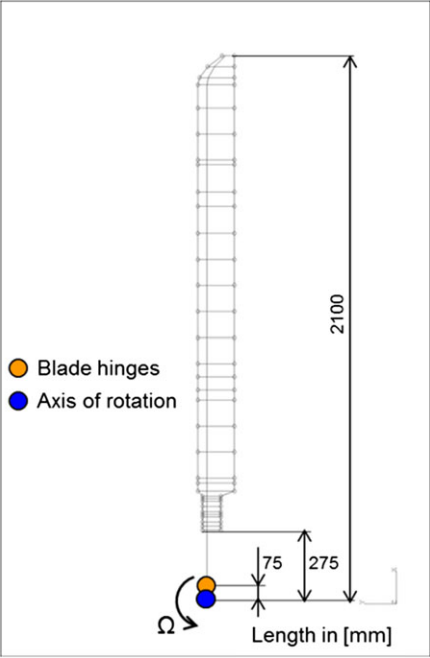


Figure 7. Finite element model with rigidly connected leading and trailing edge.

Table 3. Test cases for unsteady aerodynamic model

Case	1/Wagner	2/Wagner+	3/Wagner++
Blade aerofoil	x	x	x
Rotor inflow		x	x
Wake periodicity			x

Each rotor blade is equipped with 34 SIMPACK User Force Elements along the straight blade axis and the parabolic tip section. They provide the unsteady aerodynamic forces from circulation based on the extended Wagner function and related non-circulatory enhancements for the general motion of the aerofoil section taking heave and pitch into account. The unsteady aerodynamic contributions based on circulation include blade aerofoil, axial rotor inflow and wake periodicity from rotor blade interaction. Here, indicial functions allow to separate these effects into three cases according to Table 3 and to study their individual impact on rotor blade flutter. Similar to the previous aeroelastic assessment of the 7AD rotor [4], a pitch setting according to a blade thrust of 827N at the nominal rotor speed of 100% is chosen for the test cases.

3.2 Dynamic simulation results

The dynamic simulation results for hover are gained from the application of linearisation features in MBS SIMPACK and show the development of the rotor frequencies versus nominal rotor speed for the dynamic rotor setup. As preparatory steps, an equilibrium computation for the derivation of the dynamic model states followed by a preload computation are performed to adjust the rotor model to the chosen rotor speed. The normalised frequencies of the 7AD rotor are found in Fig. 8 and correlate well with other results [34] available inside DLR. Here, the plotted modes are numbered in ascending frequency order and the colour code describes the major motion contribution in terms of blade lag (red), flap (blue) and torsion (green) at nominal rotor speed of 100%. Hence, the mode assigned as first elastic torsion T1 represents the flap bending mode F4 for rotor speeds below the nominal operation speed, and vice versa. The dashed lines show the rotor harmonics up to 8/rev and allow the verification of the frequency placement for the 7AD dynamic rotor setup.

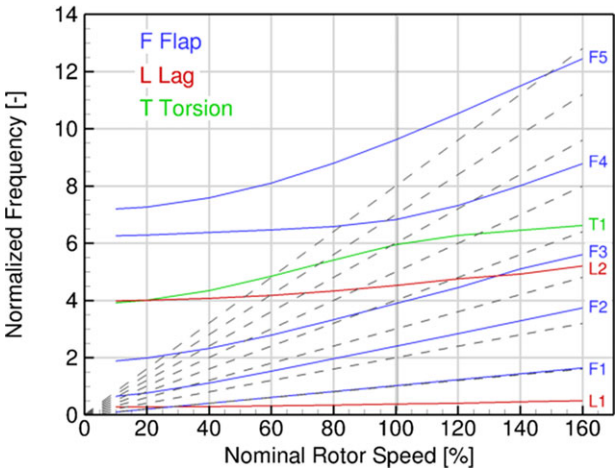


Figure 8. Rotor frequencies for the dynamic model from linearisation (aerodynamics switched off).

3.3 Aeroelastic simulation results

The aeroelastic simulation results for rotor hover are shown in Figs 9–11 and comprise the development of the 7AD rotor frequencies and natural damping versus nominal rotor speed for the three studied aeroelastic setups. Here, the used definition of natural damping is the ratio of the negative real part and the absolute value of the eigenvalues. Again, the setups are processed using available SIMPACK linearisation features together with two preceding simulation steps to derive an equilibrium for all dynamic states including indicial aerodynamics and then to preload the rotor with the appropriate aerodynamic and centrifugal loads for the chosen rotor speed. As listed in Table 3, the flutter diagrams are extracted for three test cases which differ in the unsteady aerodynamic model for circulation comprising the basic Wagner function and two extensions for axial rotor inflow and wake periodicity. Here, the unsteady motion parts from the SIMPACK User Force Element are considered by aerodynamic lag states which are found as real parts in the linearisation result and, thus, influence the blade damping. As mentioned before, the dynamic rotor setup includes a measured value for lagging damping which introduces the large damping found with both lead-lag modes L1 and L2. Similar to an earlier assessment of the 7AD rotor [4] utilising Wagner's function and apparent mass contributions for unsteady aerodynamics, a pitch setting of around 3.70° at nominal rotor speed is chosen for the three cases. Due to the refined aerodynamic modelling which is especially found in the curved region of the blade tip, the new results show some differences. These comprise a first flap bending frequency F1 which is now slightly larger than 1/rev, inverted damping values for the lead-lag modes L1 and L2 as well as a coupling of L2 with the flap bending mode F3 for large rotor speeds.

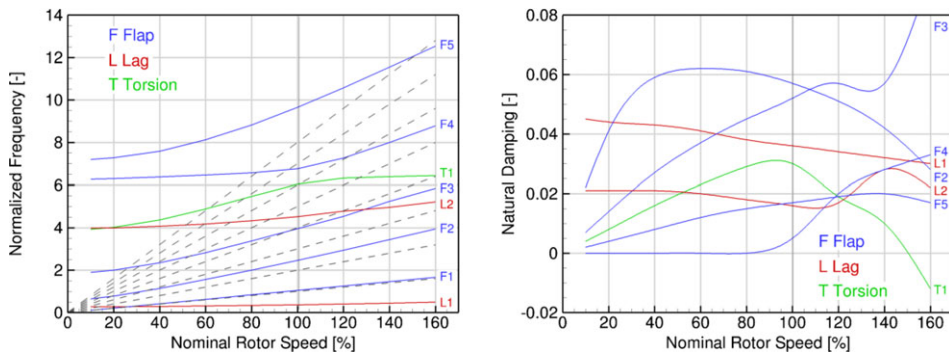


Figure 9. Rotor frequencies and damping for the aeroelastic model from linearisation (Case 1/Wagner).

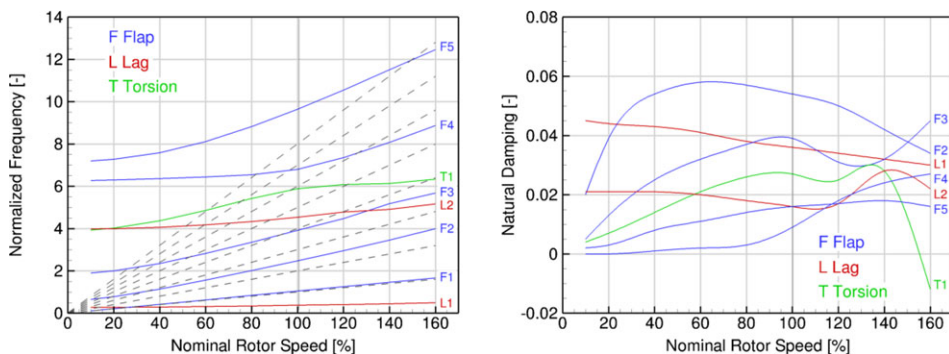


Figure 10. Rotor frequencies and damping for the aeroelastic model from linearisation (Case 2/Wagner+).

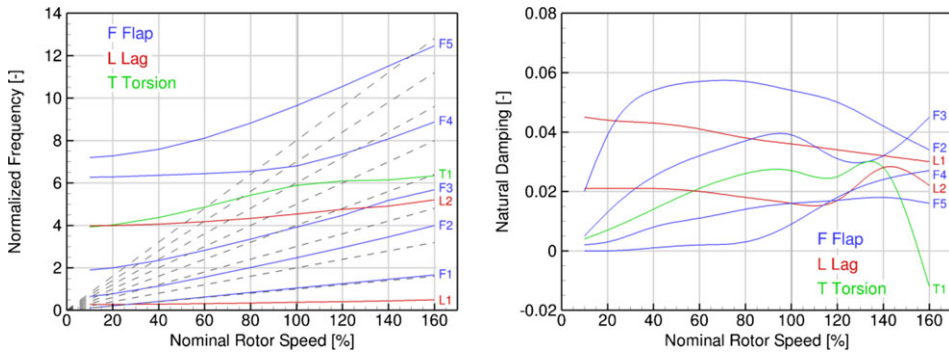


Figure 11. Rotor frequencies and damping for the aeroelastic model from linearisation (Case 3/Wagner++).

The simulation results for Case 1 based on Wagner's function and non-circulatory apparent mass consider the unsteady aerodynamic contributions for the blade aerofoil and are depicted in Fig. 9. The flutter diagrams for the aeroelastic model comprise rotor frequencies and damping. In general, both curves allow the verification of frequency placement and stability for the aeroelastic rotor system. In comparison to the rotor frequencies from the dynamic simulation as presented in Fig. 8, all bending modes show larger frequencies except for mode F4. Here, the frequency slightly decreases at 100% of nominal rotor speed and indicates an aeroelastic coupling of bending mode F4 with torsion mode T1 for which the frequency increases. Above nominal rotor speed, the frequency of T1 is decreased what indicates now a coupling with bending mode F3 towards larger rotor speeds. In contrast, the frequency curves of both lead-lag modes remain unaltered. As already implied by the frequency behaviour of the aeroelastic model, the damping curves reveal a classical bending-torsion coupling of the third flap bending mode F3 and the first torsion mode T1 as known for articulated rotor blades. This mode pair becomes unstable at 151% rotor speed. The flutter coupling can be verified by switching off F3 and then, the negative damping of mode T1 disappears. Similar to the frequency curves of F4 and T1, the damping values for flap bending mode F4 represent those of torsion T1 below the nominal operation speed, and vice versa. In addition, a slight coupling is found between flap mode F3 and lead-lag mode L2 starting around the nominal rotor speed of 120%, which remains stable. Finally, the first flap mode F1 shows very large values of natural damping of around 30% and hence, is not depicted in the plot.

The simulation results for Case 2 utilising Wagner's function, rotor inflow and non-circulatory apparent mass consider unsteady aerodynamic contributions for blade aerofoil and axial rotor inflow. The resulting flutter diagrams are found in Fig. 10, which are compared to the results of Case 1 that neglected the rotor inflow. Here, the rotor frequencies for the flap bending modes F2 and F4 show larger frequencies for Case 2, whilst the frequencies for F3, F5 and the torsion mode T1 decrease. As seen in the frequency increase of flap bending mode F4 and decrease of torsion mode T1 at 100% of nominal rotor speed, their aeroelastic coupling is less pronounced with axial inflow. Above the operation speed of 100%, the frequency of T1 is decreased which indicates again the coupling with bending mode F3 towards larger rotor speeds. All other modes comprising F1, L1 and L2 remain more or less unchanged in their frequency behaviour. As before, the damping curves reveal the bending-torsion coupling of the third flap bending mode F3 and the first torsion mode T1 with flutter onset at 158% of nominal rotor speed. As for the frequency curves of F4 and T1, the damping values for flap bending mode F4 also represent those of torsion T1 below the nominal operation speed, and vice versa. In general, the torsion mode T1 is more damped for all rotor speeds and elastic flap bending modes (F2–F5) are less damped than before, whilst damping remains rather the same for the rigid flap mode F1 as well as for both lead-lag modes L1 and L2. Again, a minor coupling of flap mode F3 and lead-lag mode L2 develops at the nominal rotor speed of 120%, which is stable within the studied speed range. Also, the flap mode F1 is

not found in the plot, since it reaches large damping values around 30%. To summarise the comparison to Case 1 in terms of rotor blade flutter in hover, it can be stated for the assessment of the 7AD rotor that the introduction of axial rotor inflow with Case 2 decreases the damping of the elastic flap bending modes, but increases torsion damping. As a result, the flutter onset is shifted to a larger rotor speed.

The simulation results for Case 3 using Wagner’s function, rotor inflow, wake periodicity and non-circulatory apparent mass consider the unsteady aerodynamic contributions for blade aerofoil, axial rotor inflow and wake periodicity. The resulting flutter diagrams from Fig. 11 are compared to those of Case 2 that do not consider wake periodicity. The obtained frequency results are the same for all modes as found before with Case 2 except for the first torsion mode T1 which shows a very small increase between the nominal rotor speeds of 120% and 140%. Also, the computed damping results are the same as known from Case 2 except for a slight decrease for flap mode F2 at 60% of nominal rotor speed. As before, the rigid flap mode F1 shows large natural damping values around 30% and is not plotted. As a summary of the comparison to Case 2, it can be stated for the flutter assessment of the 7AD rotor in hover that the added wake periodicity within Case 3 does neither change the frequency nor the damping behaviour of the aeroelastic rotor system. Hence, the flutter onset at the nominal rotor speed of 158% is the same as found for Case 2.

Finally, flutter onset gained for the three test cases of the 7AD rotor in hover is compared in Table 4. The lowest flutter onset is found for unsteady aerodynamics limited to the blade aerofoil at a nominal rotor speed of 151% (Case 1/Wagner), whilst the two other cases with added rotor inflow and wake periodicity both show flutter at 158% (Case 2/Wagner+, Case 3/Wagner++). Here, the influence of rotor inflow plays the major role, since it decreases the damping of the flap bending modes. As a consequence, the unstable torsion mode within the critical flutter coupling is increased in damping due to a weaker coupling to the participating flap mode and flutter onset is shifted to an approximately 5% larger rotor speed. For the studied 7AD rotor configuration in hover, added wake periodicity within Case 3 does neither change frequency nor damping and hence, does not affect the aeroelastic coupling in terms of a change in flutter speed.

Table 4. Flutter onset for unsteady aerodynamic models

Case	1/Wagner	2/Wagner+	3/Wagner++
Blade aerofoil	x	x	x
Rotor inflow		x	x
Wake periodicity			x
Flutter onset	151%	158%	158%

4.0 Conclusions and outlook

The experimental 7AD rotor blade was assessed for flutter stability in hover. For the aeroelastic analyses, the multibody model was tightly coupled with an unsteady aerodynamic model based on Wagner’s function and related enhancements for the general motion of an aerofoil section considering heave and pitch. Furthermore, the mathematical setup of the approximated Wagner function used in state space was extended for axial flow to include unsteady contributions related to rotor inflow and wake periodicity next to blade aerofoil. The unsteady aerodynamic model for rotor blade sections is based on indicial response functions, which capture transient changes within the Duhamel superposition integral and features a fully analytical two-dimensional airloads model. Relevant flutter diagrams are extracted in terms of frequency and damping behaviour for three test cases which differ in the aerodynamic model for circulation comprising blade aerofoil, rotor inflow and wake periodicity. Since the unsteady aerodynamic model is based on indicial response functions, a separation of these circulatory contributions is possible and allows the study of their individual impact on rotor blade flutter.

As known for articulated blades, also the straight 7AD rotor blade with parabolic blade tip exhibits the classical bending-torsion coupling. The first flutter onset is found for unsteady aerodynamics limited to the blade aerofoil at a rotor speed of 151% (Case 1/Wagner), whilst the two other cases with added rotor inflow and wake periodicity show flutter at a speed of 158% (Case 2/Wagner+, Case 3/Wagner++). Here, the influence of rotor inflow plays the major role, since it decreases the damping of the flap bending modes. As a consequence, the unstable torsion mode within the critical flutter coupling is increased in damping due to a weaker coupling to the participating flap mode and flutter onset is shifted to an approximately 5% larger rotor speed. For the studied 7AD rotor configuration in hover, added wake periodicity neither changes frequency nor damping and hence, does not affect the aeroelastic coupling in terms of a change in flutter speed.

Future investigations related to the 7AD rotor blade comprise the influence of blade tip shape and wake periodicity on the resulting aeroelastic couplings. All damping plots show a coupling between lead-lag mode L2 and flap bending mode F3 which might be related to the local dynamics and aerodynamics of the parabolic blade tip. Hence, this coupling could disappear for the rectangular 7A layout which is similar to the 7AD blade except for the curved blade tip. Furthermore, wake periodicity as modelled with the extended Wagner function does not influence the flutter speed in hover. To increase the insight into the interplay of the periodicity term from Loewy's function on unsteady lift and its consideration in the rotor blade flutter results from linearisation, future investigations will also include simulations in time domain for the further verification of the wake periodicity effect.

References

- [1] Ham, N.D. Helicopter Blade Flutter. AGARD report No. 607, 1973.
- [2] Johnson W. *Helicopter Theory*, 1st ed, Dover Publications, 1994, New York, Chapter 10.
- [3] van der Wall, B.G., Keßler, C., Delrieux, Y., Beaumier, P., Gervais, M., Hirsch, J.F., Pengel, K. and Crozier, P. From ERATO basic research to the Blue Edge™ rotor blade, American Helicopter Society 72nd Annual Forum, West Palm Beach, Florida, 2016.
- [4] Arnold, J. Flutter assessment of a rotor blade with innovative layout in hover using indicial aerodynamics, 72nd American Helicopter Society Forum, West Palm Beach, Florida, 2016.
- [5] van der Wall, B.G. Grundlagen der Dynamik von Hubschrauber-Rotoren. VDI-Buch, Springer Vieweg, 2018, Berlin, Chapter 6.
- [6] Johnson, W. Technology drivers in the development of CAMRAD II, Proc AHS Aeromechanics Specialists Conference, San Francisco, 1994.
- [7] Benoit, B., Dequin, A.M., Kampa, K., von Grünhagen, W., Basset, P.M. and Gimonet, B. HOST, a general helicopter simulation tool for Germany and France, Proc 56th AHS Annual Forum, Virginia Beach, 2000.
- [8] Yeo, H., Potsdam, M. and Ormiston, R. Application of CFD/CSD to rotor aeroelastic stability in forward flight, Proc 66th AHS Annual Forum, Phoenix, Arizona, 2010.
- [9] Morillo, J, Singh, R. and Wasikowski, M. Model development and integration of DYMORE at Bell helicopter, 64th American Helicopter Society Forum, Montréal, 2008.
- [10] Waitz, S. The structural dynamics of a free flying helicopter in MBS- and FEM-analysis, 39th European Rotorcraft Forum, Moscow, 2013.
- [11] Datta, A. and Johnson, W. Integrated aeromechanics with three-dimensional solid-multibody structures, 70th American Helicopter Society Forum, Montréal, 2014.
- [12] Weiß, F.A., Merlis, J., Lojewski, R., Hofmann, J. and Röhrig-Zöllner, M. Rotor blade modeling in a helicopter multi body simulation based on the floating frame of reference formulation, 48th European Rotorcraft Forum, Winterthur, 2022.
- [13] Lugner, P., Arnold, M. and Vaculin, O. (Eds). Vehicle System Dynamics (Special issue in memory Professor Willi Kortüm), 2004, 41, (5).
- [14] <https://www.3ds.com/products-services/simulia/products/simpack/>
- [15] Arnold, J. Flutter assessment of a rotor blade in steady axial flight based on indicial aerodynamics, 49th European Rotorcraft Forum, Bückeburg, 2023.
- [16] Schwarz, T. and Pahlke, K. CFD code validation for complete helicopters - The European GOAHEAD project, 67th American Helicopter Society Forum, Virginia Beach, Virginia, 2011.
- [17] Leishman, J.G. *Principles of Helicopter Aerodynamics*, 2nd ed, Cambridge University Press, 2006, New York, Chapter 8.
- [18] Arnold, J. and Waitz, S. Using multibody dynamics for the stability assessment of a new rotor test rig, 43rd European Rotorcraft Forum, Milan, 2017.
- [19] Arnold, J. and Waitz, S. Using multibody dynamics for the stability assessment of a new double-swept rotor blade setup, 44th European Rotorcraft Forum, Delft, 2018.
- [20] Gardner, A.D. FAST-Rescue wissenschaftlicher Ergebnisbericht. DLR Internal Report, DLR-IB-AS-GO-2020-45, 2020.

- [21] Dassault Systèmes Simulia Corp. Simpack User Assistance, 2021.
- [22] Arnold, M., Burgermeister, B., Führer, C., Hippmann, G. and Rill, G. Numerical methods in vehicle system dynamics: State of the art and current developments, *Veh. Syst. Dyn.*, 2011, **49**, (7), pp 1159–1207.
- [23] Schwertassek, R. and Wallrapp, O. *Dynamik flexibler Mehrkörpersysteme*, Vieweg, 1999.
- [24] Wallrapp O. Standardization of flexible body modeling in multibody system codes, part I: Definition of standard input data, *Mech. Struct. Mach.*, 1994, **22**, (3), pp 283–304.
- [25] Surrey, S., Ortun, B., Truong, K.V. and Wienke, F. Investigation of the structural blade dynamics and aeroelastic behavior of the 7A rotor, 72nd American Helicopter Society Forum, West Palm Beach, Florida, 2016.
- [26] Fung, Y.C. *An Introduction to the Theory of Aeroelasticity*, Dover Publications Inc, 1993, New York, Chapter 6.
- [27] Wagner, H. Über die Entstehung des dynamischen Auftriebes von Tragflügeln, *Zeitschrift für angewandte Mathematik und Mechanik*, Band 5, Heft 1, 1925.
- [28] Carpenter, P.J. and Fridovich, B. Effect of a Rapid Blade Pitch Increase on the Thrust and Induced Velocity Response of a Full-Scale Helicopter Rotor. NACA TN 3044, 1953.
- [29] Loewy, R.G. A two-dimensional approximation to the unsteady aerodynamics of rotary wings, *J. Aeronaut. Sci.*, 1957, **24**, (2), pp 81–92.
- [30] Bronstein, I.N. and Semendjajew K.A. *Taschenbuch der Mathematik*, 24th ed, BSB B.G. Teubner Verlagsgesellschaft, 1989, Leipzig, Chapter 1.1.3.
- [31] Arnold, J. Indicial aerodynamic model for flutter assessment in axial flight considering blade airfoil, rotor inflow and wake periodicity, 50th European Rotorcraft Forum, Marseille, 2024.
- [32] Miller, R.H. Rotor blade harmonic air loading, *AIAA J.*, 1964, **2**, (7), pp 1254–1269.
- [33] Hoffmann, F. and Opitz, S. Documentation for AT4 Structural Properties. Version 1.1, DLR Institute of Flight Systems, 2010.
- [34] Surrey, S, Wendisch, J.H. and Wienke, F. Coupled fluid-structure simulations of a trimmed helicopter rotor in forward flight, Proc 19th DGLR symposium STAB, Munich, 2014.